Thermodynamic Model of a Hybrid Brayton Thermosolar Plant

R.P. Merchán[a], M.J. Santos[b], A. Medina[c] and A. Calvo Hernández[d]

[a]Dpto. de Física Aplicada, University of Salamanca, 37008 Salamanca, Spain - rpmerchan@usal.es
[b]Dpto. de Física Aplicada, University of Salamanca, 37008 Salamanca, Spain - smjesus@usal.es,
[c]Dpto. de Física Aplicada, University of Salamanca, 37008 Salamanca, Spain - amd385@usal.es
[d]Dpto. de Física Aplicada University of Salamanca, 37008 Salamanca, Spain - anca@usal.es

Abstract:

We present a thermodynamic model for the prediction of the performance records of a solar hybrid gas turbine power plant. Variable irradiance and ambient temperature conditions are considered. A serial hybridization is modeled with the aim to get an approximately constant turbine inlet temperature, and thus to deliver to the grid an stable power output. The overall thermal efficiency depends on the efficiencies of the involved subsystems and the required heat exchangers in a straightforward analytical way. Numerical values for input parameters are taken from a central tower heliostat field recently developed near Seville, Spain. Real data for irradiance and external temperature are taken in hourly terms. The values of several variables at different situations are presented for a representative year: overall plant efficiency, solar conversion efficiency, solar share, power output, etc. The fuel consumption assuming natural gas is estimated, as well as greenhouse emissions. The model can be applied to predict the annual evolution of the performance of real installations in terms of a reduced set of parameters. It is also feasible to get information about the main irreversibility sources and the bottlenecks of the overall plant efficiency. This can contribute to improve the design of this kind of facilities in order to get better performance and so better economical records.

Keywords:

Thermosolar gas-turbines, Hybrid plants, Thermodynamic model, Variable solar irradiance, Global plant performance, Seasonal evolution

1. Introduction

During the last years several experimental projects have tried to develop hybrid solar gas turbine technologies in which concentrated solar power [1, 2] coming from a central receiver plant is used to heat pressurized air that performs a Brayton cycle [3, 4, 5]. This technology is suitable for regions with favorable solar irradiance conditions [6], usually linked to water shortage. These power plants can be combined with other cycles in order to improve their overall efficiency [7, 8].

The term hybrid refers to the fact that during low solar radiation periods a combustion chamber ensures a stable power release to the electricity grid and avoids the use of storage systems [9]. Several hybridization strategies have been proposed [10]. Hybridization can be performed by retrofitting an existing standard fossil plant or designing an original hybrid one [11]. Usually there is more flexibility in designing and optimizing a brand new one, solving the design challenges properly. It is thus required to simulate the hybrid system, taking into account technological, thermodynamic, and economic ingredients [7, 10, 12]. For design purposes it is usual to choose particular stationary conditions for solar irradiance and ambient temperature. Sometimes these design point conditions are too optimistic and do not properly reflect the fluctuating behavior due to daily and seasonal changes of solar irradiance at a particular place.

Apart from R+D projects, prototypes, and experimental installations several research works have been published in the last times. Some of them make use of commercial simulation environments or in-house developed software which allows a detailed description of all plant components and specific calculations on the solar subsystem [3, 13]. With respect to the latter, exhaustive computations for the solar efficiency including mirror area, spillage, blocking and shadowing effects, mirror tracking strategies, and so on are accomplished [14, 15]. These simulations rely on

the detailed model of each plant component, thus leading to a large amount of parameters to be simultaneously optimized which is a difficult task. So, it is not easy to extract direct physical information about the main losses sources in the plant and to plan global strategies for the optimization of the plant design and operation as a whole.

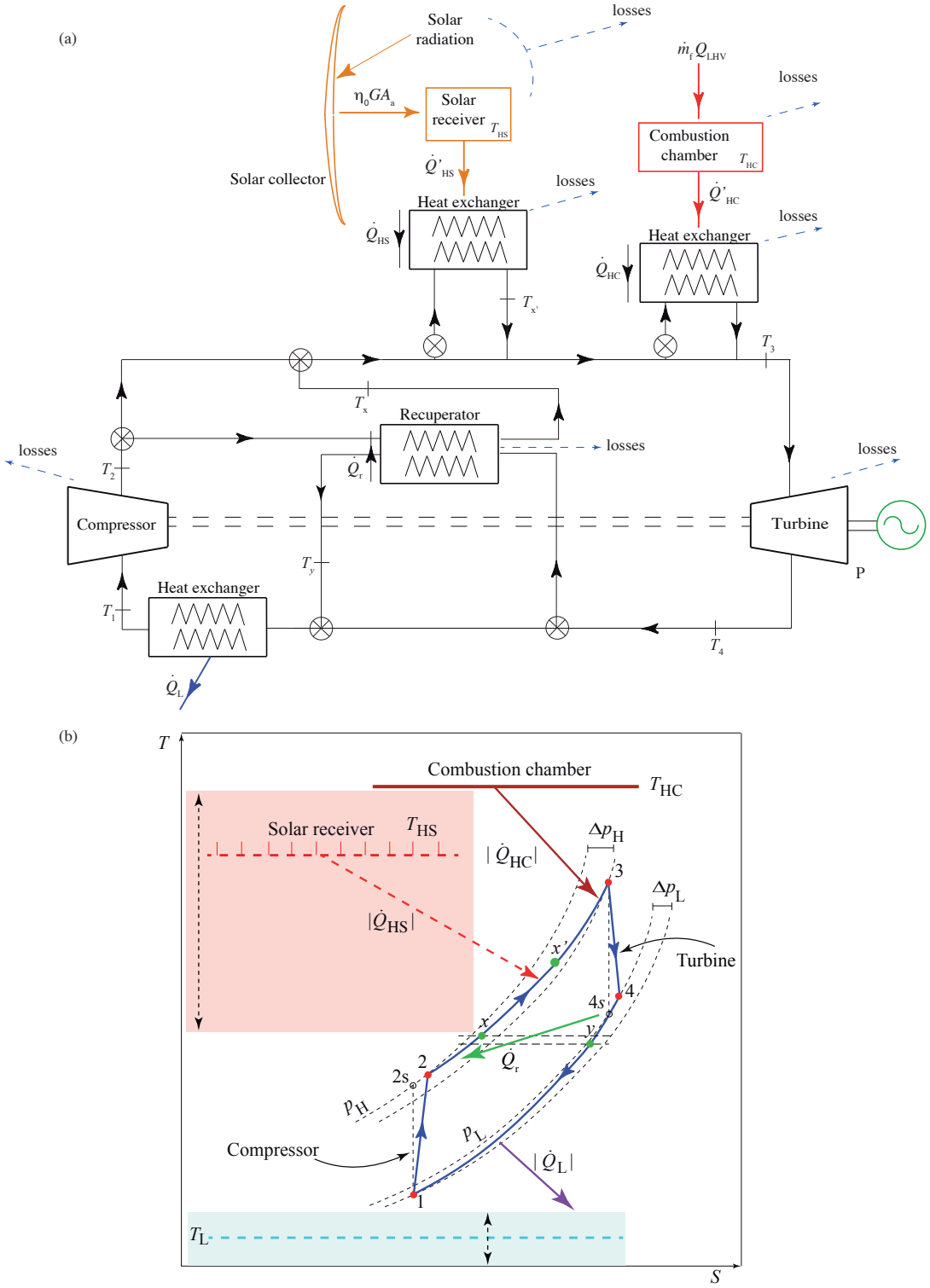

Figure 1: (a) Scheme of the hybrid solar gas-turbine plant considered. The main heat transfers and temperatures are depicted. Also the key losses sources considered in the model are shown. (b) $T-S$ diagram of the irreversible Brayton cycle experienced by the working fluid.

On the other side, there are several theoretical works starting from the Brayton ideal cycle. Thereafter refinements are included in cycle thermodynamics in order to recover realistic output records [16, 17, 18]. Usually, in these works the model for the concentrated solar subsystem, although including the main heat transfer losses, is simple. This favors to obtain closed analytical expressions for thermal efficiencies and power output, and then check the model predictions for particular design point conditions, with fixed values of solar irradiance and ambient temperature. And in a possible step forward to suggest and guide optimization strategies.

Within the last *modus operandi*, we present a thermodynamic cycle that starts from a closed Brayton cycle however incorporating the main losses sources: non-ideal turbine and compressor, pressure decays, heat exchangers, heat transfer losses in the solar collector, combustion inefficiencies, etc. The model is flexible and allows to check the performance of several plant configurations. Special emphasis will be done on recuperation because of its key influence on the plant output records [6, 19, 20]. The model is dynamic in which refers to solar irradiance and ambient temperature. It allows to obtain curves for any plant output record in terms of those parameters and analyze hourly and seasonal changes at any particular location.

The combination of the models for the solar part and the thermodynamic engine leads to expressions for the plant global efficiency and other performance data in terms of a reduced number of parameters, with clear physical meaning each. This is a basic pre-design simulation scheme in order to understand the main bottlenecks to consider in the design of this kind of facilities. It will be shown that the comparison of the model predictions with real plant data at particular conditions is good. Moreover, we shall present a complete analysis of the evolution of plant records along a year, taking real measurements for solar irradiance and ambient temperature for representative days of each season. Particularly, fuel consumption and greenhouse emissions will be estimated and analyzed.

2. Thermodynamic plant model

We consider a central tower solar installation as sketched in Fig. 1(a). A single step recuperative closed Brayton cycle is hybridized in order to obtain a stable power output, independent of the solar irradiance conditions. The design is flexible because the plant can work in different modes: with or without solar hybridization depending on irradiance conditions, and with or without recuperator. Next we briefly describe the main thermodynamic processes experienced by the working fluid. The working fluid at the compressor exit (temperature T_2) is heated up through a recuperator that makes use of the high temperature of the gas after the turbine, T_4. The temperature of the fluid at the recuperator exit, T_x, is elevated first by the heat released by the central tower solar subsystem if solar irradiance is enough. Afterwards, the fluid reaches a higher temperature, $T_{x'}$ and then, in the last heating step, it receives an energy input from a combustion chamber through another heat exchanger. The final temperature at the turbine inlet, T_3, is taken as approximately constant, so the power released by the installation to the grid is stable. In the case of insufficient irradiance a shut-off valve redirects the fluid directly to the heat exchanger below the combustion chamber.

Next we detail the nomenclature for the different heat transfers in the model. The solar subsystem receives a heat input from the sun given by GA_a where G is the direct solar irradiance and A_a the aperture area of the solar field. The solar irradiance is a function of time because it depends on the sun position during the day, weather conditions, and seasonal fluctuations. After discounting the losses, the receiver releases a useful energy to a heat exchanger, $\dot{Q}'_{HS}$, that in turn releases a final heat rate $\dot{Q}_{HS}$ to the working fluid.

A similar scheme is followed to describe the combustion chamber subsystem. The energy input in this subsystem is $\dot{m}_f Q_{LHV}$, where $\dot{m}_f$ is the fuel mass consumption rate and Q_{LHV} its corresponding lower heating value. The mass fuel rate will be also considered as time dependent, in accordance to the fluctuations of G. It should compensate variations in G in such a way that the turbine inlet temperature remains approximately constant in all conditions. In the combustion chamber losses

due to incomplete combustion and heat transfers to the surroundings are accounted for. The heat rate received by the working fluid from combustion of the fuel is denoted as $\dot{Q}_{HC}$. The effectivenesses of the heat exchangers associated to the solar and the combustion subsystems are denoted as ε_{HS} and ε_{HC} respectively. The internal heat transfer associated to recuperation is called $\dot{Q}_r$. In order to close the thermodynamic cycle a cold-side heat exchanger is considered. The compressor inlet temperature, T_1, will depend on the external temperature, T_L, that will fluctuate due to daily and seasonal changes. Thus, all other temperatures in the cycle will oscillate because of the same reasons. The plant delivers a mechanical power output, P, independent of solar radiation fluctuations.

2.1. Global thermal efficiency of the plant

The thermal efficiency of the whole system, η, is the ratio between the net mechanical power output, P, and the total heat input rate,

$$\eta = \frac{P}{GA_a + \dot{m}_f Q_{LHV}}. \qquad (1)$$

The following objective is to express this global efficiency in terms of the efficiency of the solar collector, η_S, that of the combustion chamber, η_C, the efficiency of the Brayton heat engine, η_H, and the effectivenesses of all the required heat exchangers. Details of the calculations can be found in [18]. The overall efficiency of the whole system, η, is obtained as:

$$\eta = \eta_S \eta_C \eta_H \left[\frac{\varepsilon_{HS}\varepsilon_{HC}}{\eta_C \varepsilon_{HC} f + \eta_S \varepsilon_{HS}(1-f)}\right]. \qquad (2)$$

This expression is valid for the hybrid mode when both heat sources are simultaneously releasing energy to the fluid. In the particular case in which eventually all the energy input comes from the solar collector, $f = 1$, and $\eta = \eta_S \eta_H \varepsilon_{HS}$, and when solar irradiance is null, and the turbine works only with the heat released in the combustion reactions, $f = 0$, and $\eta = \eta_C \eta_H \varepsilon_{HC}$.

It is also interesting to define a performance relative to the energy input with an economical cost, i.e., to the fuel burned. It constitutes a *fuel conversion rate*, and can be defined as, $r_e = P/\left(\dot{m}_f Q_{LHV}\right)$. It is easy to show that:

$$r_e = \frac{\eta \eta_S \eta_H \varepsilon_{HS}}{\eta_S \eta_H \varepsilon_{HS} - \eta f}. \qquad (3)$$

In the particular case all the energy input comes from combustion, $f = 0$, and $r_e = \eta$. In the opposite limit, if eventually all the energy was solar, $f = 1$, and $\eta = \eta_S \eta_H \varepsilon_{HS}$, so $r_e \to \infty$.

2.2 Solar subsystem and combustion process efficiencies

We consider a simple model for the concentrating solar system in order to be able to obtain analytical closed expressions for the overall plant efficiency. At low and intermediate working temperatures for the solar collector, T_{HS}, losses essentially comes from conduction and convection. At high temperatures radiation losses become significant and should be considered in any model. The energy collected at the aperture is GA_a, and the useful energy provided by the solar plant, $\left|\dot{Q}'_{HS}\right|$, is the difference between the energy transmitted to the receptor, $\eta_0 GA_a$ and the losses. η_0 is the effective optical efficiency considering losses coming from spillage, shadowing, blocking, sun position effects, and so on. Thus, the useful heat released from the collector and its efficiency can be respectively expressed, as [22, 23]:

$$\left|\dot{Q}'_{HS}\right| = \eta_0 GA_a - \alpha\sigma A_r T_L^4(\tau_{HS}^4 - 1) - U_L A_r T_L(\tau_{HS} - 1), \qquad (4)$$

$$\eta_S = \frac{\left|\dot{Q}'_{HS}\right|}{GA_a} = \eta_0[1 - h_1 T_L^4(\tau_{HS}^4 - 1) - h_2 T_L(\tau_{HS} - 1)]. \qquad (5)$$

In (4) and (5), $\tau_{HS} = T_{HS}/T_L$ denotes the ratio between the working temperature of the solar receiver, T_{HS}, and the surroundings, T_L. A_a and A_r are, respectively, the aperture and absorber areas, $h_1 = \alpha\sigma/(\eta_0 GC)$, $h_2 = U_L/(\eta_0 GC)$ are losses parameters, where U_L is the convective heat loss coefficient, α is the effective emissivity of the collector, $C = A_a/A_r$ is the concentration ratio, and σ the Stefan-Boltzmann constant. It will be considered in our model that the direct solar irradiance, G, and the surroundings temperature, T_L, are time functions because oscillate during a day and change with seasonal and meteorological conditions. For each particular pair of values of G and T_L at any given instant, the working temperature of the receiver, T_{HS}, is calculated by balancing the energy received from the sun and that released to the working fluid experiencing the bottoming thermal cycle [17]. The heat released by the solar subsystem to the working fluid is $|\dot{Q}_{HS}| = \varepsilon_{HS}|\dot{Q}'_{HS}|$, where $\varepsilon_{HS} = (T_{x\prime} - T_x)/(T_{HS} - T_x)$.

The efficiency of the combustion chamber, η_C, once elected the fuel to be burned and the fuel-air equivalence ratio, can be considered as a constant parameter. In real equipment it could slightly change with fluctuations of the fuel-air equivalence ratio, the composition of the fuel, its temperature, and several other variables, but we are more interested in an adequate qualitative description. The heat received by the working fluid from the combustion chamber, $\dot{Q}_{HC}$, can be written as:

$$|\dot{Q}_{HC}| = \varepsilon_{HC}|\dot{Q}'_{HC}| = \varepsilon_{HC}\eta_C\dot{m}_f Q_{LHV}. \qquad (6)$$

By expressing the effectiveness of the heat exchanger in between the combustion chamber and the thermal cycle as (see Fig. 1) $\varepsilon_{HC} = (T_3 - T_{x\prime})/(T_{HC} - T_{x\prime})$, the heat released, in terms of temperatures, is:

$$|\dot{Q}_{HC}| = \dot{m}c_\omega(T_3 - T_{x\prime}) = \dot{m}c_\omega\varepsilon_{HC}(T_{HC} - T_{x\prime}), \qquad (7)$$

where $\dot{m}$ is the working fluid mass flow and c_ω is its specific heat. The effective temperature in the combustion chamber is denoted as T_{HC}, and the associated temperature ratio as $\tau_{HC} = T_{HC}/T_L$. As fluctuations in G and T_L will be taken into account, the fuel mass flow to be burned in the combustion chamber will also be a time dependent function in general given by:

$$\dot{m}_f = \frac{\dot{m}c_\omega(T_3 - T_{x\prime})}{\eta_C Q_{LHV}\varepsilon_{HC}}, \qquad (8)$$

where $T_{x\prime}$ will vary with the solar irradiance and ambient conditions. The rate of fuel mass burned can be also obtained from the fuel conversion rate, r_e, as: $\dot{m}_f = P/(r_e Q_{LHV})$.

2.3 Brayton gas-turbine efficiency

In this subsection the main assumptions considered for evaluating the efficiency of the heat engine, η_H, will be briefly outlined since the model has been detailed elsewhere in previous works by our group [18, 20]. It is assumed that a mass rate of an ideal gas, $\dot{m}$, with temperature dependent specific heat, $c_\omega(T)$, undergoes an irreversible closed recuperative Brayton cycle. The $T - S$ diagram of the cycle is depicted in Fig. 1(b), where it is stressed that both the working temperature of the solar receiver, T_{HS} and that of the surroundings, T_L, are fluctuating quantities.

1. As starting step the gas is compressed $(1 \rightarrow 2)$ by means of a non-ideal compressor. Its isentropic efficiency is given by $\varepsilon_c = (T_{2s} - T_1)/(T_2 - T_1)$. In this equation T_{2s} represents the temperature of the working fluid after the compression process if it was adiabatic and T_2 is the actual temperature at the compressor outlet.
2. Between states 2 and 3, in the most general situation, the gas receives three energy inputs in sequence. First, the non-ideal recuperator increases the gas temperature from T_2 to T_x. Its effectiveness, ε_r, is defined as the ratio between the actual temperature $(T_x - T_2)$ increase and the maximum ideal one $(T_4 - T_2)$: $\varepsilon_r = (T_x - T_2)/(T_4 - T_2) = (T_y - T_4)/(T_2 - T_4)$. In the case of a non-recuperative cycle, $\varepsilon_r = 0$, and in the ideal limit, $\varepsilon_r = 1$.

   Secondly, the gas receives a heat flow, $|\dot{Q}_{HS}|$, from the solar subsystem (step $x \rightarrow x'$) and thus its temperature increases from T_x to $T_{x\prime}$. Finally, the gas receives a completing heat input from the

combustion chamber $(x' \rightarrow 3)$ in order to ensure an approximately constant turbine inlet temperature, T_3, independently of the solar irradiance conditions.

In which respect to the pressure during the heat addition processes, a global parameter, ρ_H, that quantifies the pressure decrease in the process $2 \rightarrow 3$ is considered. In real plants pressure decays are associated to the particular equipment in any of the three steps of the heat input process, so the curve $2 \rightarrow 3$ would not be as smooth as it is plotted in Fig. 1(b). But the consideration of a unique global pressure decay parameter allows to obtain analytical equations and to numerically check the effects of pressure decays in the output parameters of the plant [13]. This parameter, ρ_H, is defined as:

$$\rho_H = \frac{p_H - \Delta p_H}{p_H}, \qquad (9)$$

where p_H is the highest pressure of the gas and $(p_H - \Delta p_H)$ its pressure at the turbine inlet.

3. In the state 3 the working fluid has reached its maximum temperature and its is expanded by means of a non-ideal turbine performing the power stroke $(3 \rightarrow 4)$. In Fig. 1(b) the state $4s$ represents the final state in the ideal case the turbine behaves isentropically, and the state 4 is the actual final state after expansion. The isentropic efficiency of the turbine, ε_t, is given by: $\varepsilon_t = (T_4 - T_3)/(T_{4s} - T_3)$.
4. Lastly, the gas recovers the conditions at the initial state 1 by releasing heat in the process $4 \rightarrow 1$ through two steps. First, by means of the recuperator (process $4 \rightarrow y$) and later by exchanging heat to the ambient through a non-ideal heat exchanger with effectiveness, ε_L (process $y \rightarrow 1$): $\varepsilon_L = \big(T_1 - T_y\big)/\big(T_L - T_y\big)$.

   The pressure loss during the whole heat release process is measured through a coefficient ρ_L given by:

$$\rho_L = \frac{p_L - \Delta p_L}{p_L}, \qquad (10)$$

   where p_L is the gas pressure at the turbine outlet and $(p_L - \Delta p_L)$ its lowest pressure during the cycle. It is convenient to define a global pressure ratio, r_p as:

$$r_p = \frac{p_H}{p_L - \Delta p_L}. \qquad (11)$$

   Provided that the processes $1 \rightarrow 2s$ and $3 \rightarrow 4s$ are adiabatic (see Fig. 1(b)), two parameters, a_c and a_t, related to the pressure ratios of the compressor and the turbine respectively are defined:

$$a_c = \frac{T_{2s}}{T_1} = \left(\frac{p_H}{p_L - \Delta p_L}\right)^{(\bar{\gamma}_{12}-1)/\bar{\gamma}_{12}} = r_p^{(\bar{\gamma}_{12}-1)/\bar{\gamma}_{12}}, \qquad (12)$$

$$a_t = \frac{T_3}{T_{4s}} = \left(\frac{p_H - \Delta p_H}{p_L}\right)^{(\bar{\gamma}_{34}-1)/\bar{\gamma}_{34}}, \qquad (13)$$

   where $\bar{\gamma}_{12}$ is the average adiabatic coefficient in the compression process and $\bar{\gamma}_{34}$ the corresponding one during expansion.

   Then, from (9) and (10):

$$\frac{p_H - \Delta p_H}{p_L} = \rho_H \rho_L r_p, \qquad (14)$$

   and so:

$$a_t = \left(\rho_H \rho_L r_p\right)^{(\bar{\gamma}_{34}-1)/\bar{\gamma}_{34}}. \qquad (15)$$

   Both coefficients, a_t and a_c are not independent, both are related through the pressure ratio, r_p.

Once, the main hypothesis and parameters have been made explicit, we express the temperatures of all the states in the cycle in terms of the temperature of the solar collector, T_{HS}, that of the combustion chamber, T_{HC}, and the pressure ratios of the compressor, a_c and the turbine, a_t. By using the definitions in the section above, it is possible to obtain the following set of equations:

$$T_1 = \varepsilon_L T_L + T_y(1 - \varepsilon_L), \qquad (16)$$

Table 1: Simulation predictions for the main parameters of the hybrid solar gas-turbine plant developed for the SOLUGAS project [5, 26]. The elected parameters for the simulation of the combustion chamber and solar subsystems can be found in [18].

Solar plant parameters at design point		
$\eta_0 = 0.65$	$\varepsilon_{HS} = 0.78$	$G = 860$ W/m^2
$\alpha = 0.1$	$C = 425.2$	$U_L = 5$ W/(m^2 K)
Combustion related parameters		
$\eta_C = 0.98$	$T_{HC} = 1430$ K	$\varepsilon_{HC} = 0.98$
Thermal cycle temperatures (K)		
$T_1 = 294$	$T_2 = 590$	$T_x = 822$
$T_{x'} = 1027$	$T_3 = 1422$	$T_4 = 890$
$T_y = 657$		
Estimated output parameters		
$f = 0.341$	$\dot{m}_f = 0.172$ kg/s	$P = 4.647$ MW
Estimated efficiencies		
$\eta_H = 0.393$	$\eta_S = 0.698$	$\eta = 0.300$

$$T_2 = T_1 + \frac{1}{\varepsilon_c}(T_{2s} - T_1) = T_1 Z_c, \quad (17)$$

$$T_3 = \varepsilon_{HC} T_{HC} + T_{x'}(1 - \varepsilon_{HC}), \quad (18)$$

$$T_4 = T_3 - \varepsilon_t (T_3 - T_{4s}) = T_3 Z_t, \quad (19)$$

$$T_x = \varepsilon_r T_4 + T_2(1 - \varepsilon_r), \quad (20)$$

$$T_y = \varepsilon_r T_2 + T_4(1 - \varepsilon_r), \quad (21)$$

$$T_{x'} = \varepsilon_{HS} T_{HS} + T_x(1 - \varepsilon_{HS}). \quad (22)$$

Equations (17) and (19) were simplified by introducing two definitions:

$$Z_c = 1 + \frac{1}{\varepsilon_c}(a_c - 1), \quad (23)$$

$$Z_t = 1 - \varepsilon_t \left(1 - \frac{1}{a_t}\right), \quad (24)$$

By simultaneously using (16)-(22) it is feasible to express all the temperatures in terms of the temperatures of the heat sources, T_{HS} and T_{HC}, the ambient temperature, T_L, the pressure ratio, r_p and all the irreversibility parameters defined above. The following closed set of expressions is obtained:

$$T_2 = \frac{(1-\varepsilon_L)(1-\varepsilon_r)[\varepsilon_{HC} T_{HC} + \varepsilon_{HS} T_{HS}(1-\varepsilon_{HC})] + \varepsilon_L T_L [Z_t^{-1} - (1-\varepsilon_{HC})(1-\varepsilon_{HS})\varepsilon_r]}{[Z_c^{-1} - (1-\varepsilon_L)\varepsilon_r][Z_t^{-1} - (1-\varepsilon_{HC})(1-\varepsilon_{HS})\varepsilon_r] - (1-\varepsilon_{HC})(1-\varepsilon_{HS})(1-\varepsilon_L)(1-\varepsilon_r)^2}, \quad (25)$$

$$T_4 = \frac{[\varepsilon_{HC} T_{HC} + \varepsilon_{HS} T_{HS}(1-\varepsilon_{HC})][Z_c^{-1} - (1-\varepsilon_L)\varepsilon_r] + \varepsilon_L T_L (1-\varepsilon_{HC})(1-\varepsilon_{HS})(1-\varepsilon_r)}{[Z_c^{-1} - (1-\varepsilon_L)\varepsilon_r][Z_t^{-1} - (1-\varepsilon_{HC})(1-\varepsilon_{HS})\varepsilon_r] - (1-\varepsilon_{HC})(1-\varepsilon_{HS})(1-\varepsilon_L)(1-\varepsilon_r)^2}. \quad (26)$$

It is easy to get all the temperature of the working fluid by substituting (25) and (26) in (16)-(22). The total heat input rate, $|\dot{Q}_H|$, and, the heat release, $|\dot{Q}_L|$, are expressed in terms of the temperatures in the following way:

$$|\dot{Q}_H| = |\dot{Q}_{HS}| + |\dot{Q}_{HC}|, \quad (27)$$

$$|\dot{Q}_L| = \dot{m} \int_{T_1}^{T_y} c_\omega(T) dT, \quad (28)$$

where,

$$|\dot{Q}_{HS}| = \dot{m} \int_{T_x}^{T_{x'}} c_\omega(T) dT = f|\dot{Q}_H|, \quad (29)$$

$$|\dot{Q}_{HC}| = \dot{m} \int_{T_{x'}}^{T_3} c_\omega(T) dT = (1-f)|\dot{Q}_H|. \quad (30)$$

In these equations $c_\omega(T)$ represents the temperature dependent constant pressure specific heat of the working fluid. Thus, the power output released by the heat engine, $P = |\dot{Q}_H| - |\dot{Q}_L|$ and its thermal efficiency, $\eta_H = P/|\dot{Q}_H|$, have analytical expressions susceptible to be evaluated for any particular parameters arrangement. And so, from the considered models for the solar and the combustion chamber subsystems, it is possible to obtain the overall plant efficiency from (2).

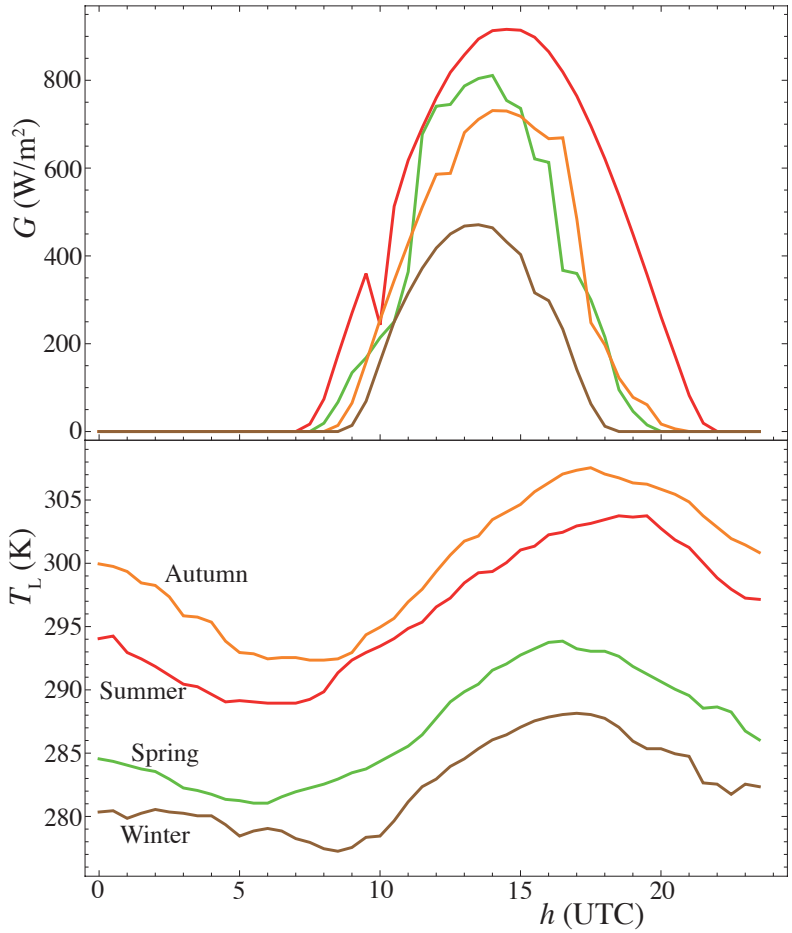

Figure 2: Hourly direct irradiance, G, and ambient temperature, T_L, for four selected days at the beginning of each season at Seville [28]. Curves are neither smoothed nor averaged.

3. Numerical implementation

3.1. Validation at design point conditions

The model presented in this work was validated for fixed solar irradiance conditions in previous works [17, 18]. In this section we outline the main background and conclusions of the numerical validation. As validation target it was elected the central tower concentrating collector developed by Abengoa Solar near Seville, Spain, under the project called SOLUGAS [5]. The turbine used in the project is the model *Mercury 50* from Caterpillar, for which the manufacturer provides several specifications [24]. The predictions of our model for this turbine were validated in [17, 18] and the agreement is quite satisfactory. Dry air was considered as working fluid, with polynomial fits for constant pressure specific heat taken from [25]. All the parameters required to obtain the numerical predictions can be found in [17, 18].

Table 1 contains some parameters of the solar subsystem of the project SOLUGAS [5] as well as the predictions from our model at fixed design conditions. For the lower heating value of natural gas a value of $Q_{LHV} = 47.141$ MJ/kg [27] was taken. The estimated efficiencies shown at the bottom of Table 1 are in right accordance with published values for this kind of plants [2, 26]. The fuel conversion rate predicted is $r_e = 0.573$.

3.2. Daily and seasonal variations of solar irradiance and ambient temperature

Direct irradiance, G, and ambient temperature, T_L, were taken from the database by Meteosevilla [28] at a location very close to the installation of the project SOLUGAS, Sanlúcar La Mayor, Seville, Spain. We took data from four regular days in 2013, each corresponding to the beginning of a season (21st): March, June, September, and December. Data were taken every 30 minutes. No smoothing or averaging procedures were followed. The curves for G and T_L are represented in Fig. 2. Seville has a priori quite favorable solar conditions. The upper panel of the figure shows that the maximum value of G reached in summer is about 875 W/m^2. The maximum of the less favorable month, december reaches about 480 W/m^2. The number of insolation hours is quite elevated. At the same time ambient temperatures are relatively high. They reach maximum values around 34ºC during the day in september (in september, at the end of summer, temperatures are higher than in june) and minimum values about 4ºC.

For each pair of values of G and T_L the working temperature of the collector, T_{HS} was calculated. All the results presented in this work were obtained from our own software, developed in programming language Mathematica®. In the next sections, results with plant configurations either incorporating a recuperator or not will be shown. When no recuperator is included, investments costs are reduced, thermal efficiency decreases, and fuel consumption is higher. But temperature of the working fluid at the exit of the expansion process is high and so, the cycle is susceptible to be combined with a bottoming cycle. In the opposite situation, when an extra investment is made in the plant and a recuperator is incorporated in the design, fuel costs decrease and thermal efficiency increases, but the temperature at the recuperator exit could make more difficult to use residual heat for bottoming cycles. Moreover, the inclusion of a recuperator will be only beneficial for not too high values of the compressor pressure ratio as discussed elsewhere in the literature [6, 19, 20].

4 Model predictions

4.1 Plant efficiencies

We have obtained the curves for the different thermal plant efficiencies and solar share for a representative day of each season in terms of the UTC time for two plant configurations (see Fig. 1): recuperative ($\varepsilon_r = 0.775$) and non-recuperative ($\varepsilon_r = 0$). These efficiencies are plotted in Fig. 3 (no recuperation is considered) and 4 (including a recuperator). The efficiency of the solar subsystem, η_S, is only defined when the solar irradiance is enough to deliver an effective heat to the working fluid, so the corresponding curves are set out for a particular time interval. For any season these curves present a wide plateau during the hours with good insolation and then η_S decreases during sunrise and sunset. The shape of the functions in these periods is only indicative because a particular model for the evolution of the solar receiver temperature with G during transients should be necessary. This is out of the scope of this work. The plateaus are associated to the fact that solar efficiency is governed by the optical efficiency, η_0, that we considered as constant. The influence of heat losses is small in the shape of η_S, specially in the non-recuperative case (see Fig. 3), only the height of the plateaus is sensitive to the temperature dependent heat losses, (5). Of course the plateaus are wider during summer, because of the higher number of insolation hours. Largest values of η_S are about 0.63 for the non-recuperative case and slightly smaller for the recuperative case. This is due to the fact that working temperatures of the solar collector are higher in this case and so heat transfer losses in the solar subsystem are larger.

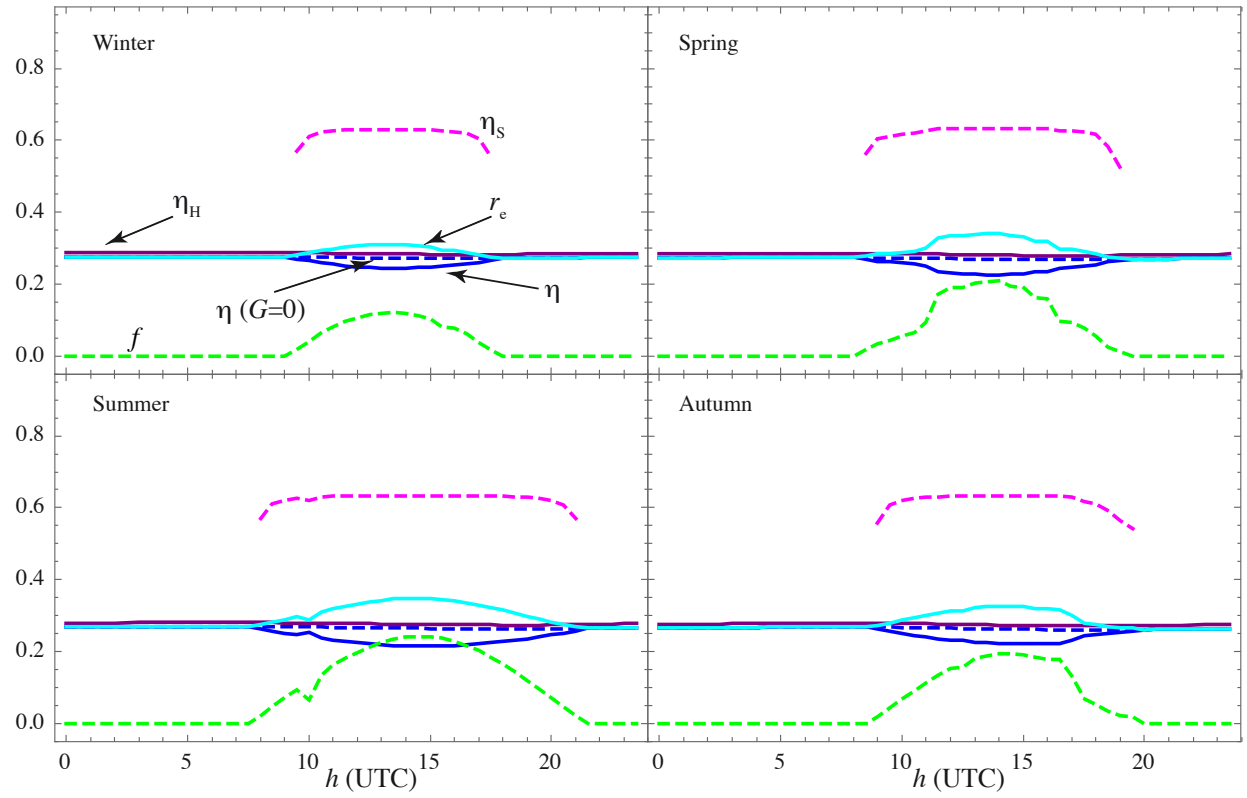

Figure 3: Hourly evolution of plant efficiencies and solar share, f, for representative days of each season. The plant configuration does not include a recuperator.

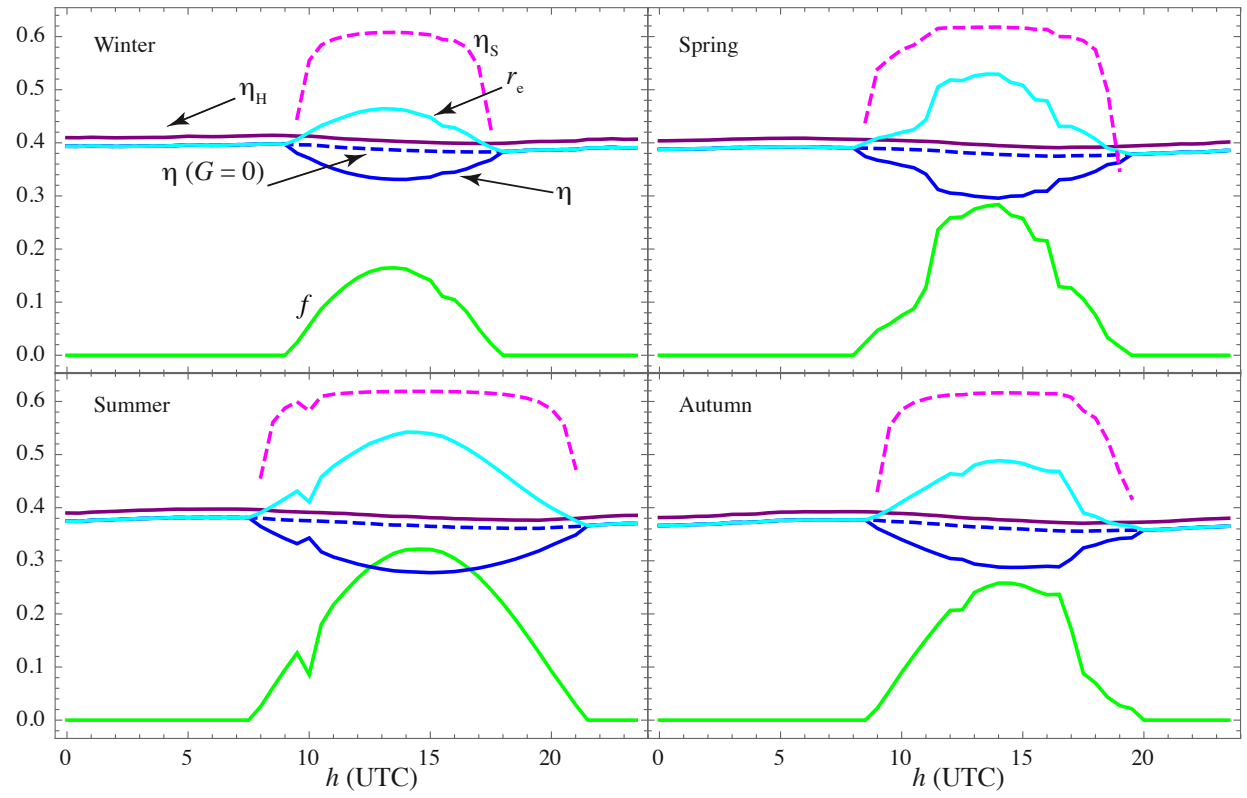

Figure 4: Hourly evolution of plant efficiencies and solar share, f, for representative days of each season. The plant configuration includes a recuperator with effectiveness $\varepsilon_r = 0.775$.

The efficiency of the Brayton heat engine, η_H, is almost constant, day and night. It depends on the ambient temperature for a particular day but its time dependence is small in the scale of the plots in Figs. 3 and 4. In seasonal terms, η_H, is higher for lower ambient temperatures: winter and spring. Its numerical value significantly increases when incorporating a recuperator, as it should be expected. For instance in winter, in Fig. 3, it amounts approximately 0.29 and in Fig. 4 increases up to 0.41. This represents an increase about 41% which is very significant. The relative increase is approximately the same in all seasons.

The global plant efficiency, η, appears as a combination of η_S, η_H, the efficiency of the combustion process, η_C, and the effectivenesses of heat exchangers (see (2)). In the absence of insolation, η, is almost time independent and becomes close to η_H. Numerical differences appear due to the combustion inefficiencies and heat exchanger losses. When the solar receiver begins its contribution as G increases, the solar subsystem is coupled to the turbine and the combustion chamber and so, the global efficiency decreases: it presents a dip during the central hours of the day. The well width depends on the number insolation hours and its depth of the maximum values that G reaches. In the recuperative configuration, Fig. 4, of course numerical values of η are larger than for the non-recuperative, Fig. 3, one because of the important increase of η_H. For $\varepsilon_r = 0$, minimum values of η change between 0.21 in summer to 0.24 in winter. For $\varepsilon_r = 0.775$ the smallest value is found in summer, 0.28, and in winter is around 0.33.

Although the fuel conversion rate, r_e, thoroughly is not a thermal efficiency is also plotted in Figs. 3 and 4. It is identical to η during nights because all the heat input is associated to fuel combustion and during the day it has a parabolic shape that resembles the shape of G and qualitatively is like a mirror image of η. The maximum value of r_e appears in summer, when irradiance reaches its higher values: for $\varepsilon_r = 0$. It amounts 0.35 and for $\varepsilon_r = 0.775$, 0.54 which is a quite interesting value. In the less favorable season, winter, it amounts 0.31 without recuperation and 0.46 with recuperation.

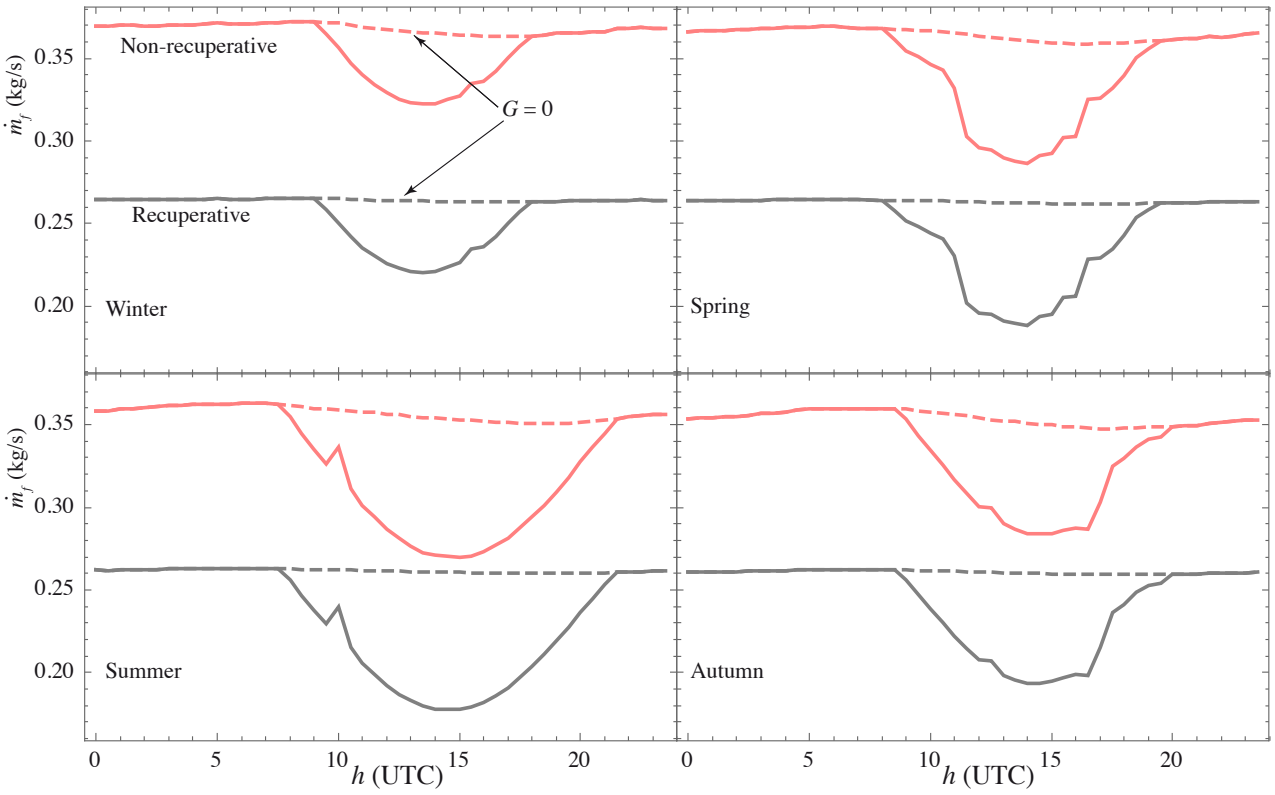

Figure 5: Evolution with time of the fuel consumption rate, $\dot{m}_f$, supposed natural gas for representative days of each season. Solid lines refer to the hybrid operation mode and dashed ones to the pure combustion mode.

The solar share, *f*, was defined in Sec. 2 as the ratio between the input heat rate from the solar collector and the total input heat rate. Its evolution with time for the considered representative days is plotted in Fig. 3 (non-recuperative) and Fig. 4 (recuperative). In all cases the shape of *f* for any particular season reminds that of the solar irradiance, *G*. Differences among seasons refer both to the number of hours with enough solar irradiance and to the height of the curves maxima. For instance in winter for the recuperative configuration *f* reaches a value slightly above 0.16 and there are 9 hours of effective irradiance. At the other side, for a typical day of summer, f has a maximum around 0.32 and about 14 hours of adequate solar input. When the recuperator is eliminated, for example, with the aim to take advantage of the residual heat in a bottoming cycle, the solar heat input remains the same. Nevertheless, the total heat input (in this case required to increase the temperature from T_2 to T_3 instead of from T_x to T_3) is larger, so the solar share is smaller. If we compare *f* in the figure for winter in both configurations, in the recuperative one the maximum is about 0.165 as mentioned above and for the non-recuperative one about 0.121. This corresponds to a decrease around 36%. At the other end, in summer the maximum with no recuperation is on 0.241, thus an increase about 34% is gained with a recuperator.

4.2 Fuel consumption and emissions

Numerical computation of the fuel consumption was achieved, either calculating the fuel consumption rate in hourly basis through (8) or the integrated consumption during a whole day. The mass fuel rate, $\dot{m}_f$, (see Fig. 5) has two different levels depending on the plant configuration, with or without a heat recuperator. During the night all the electricity generation comes from fuel combustion (natural gas in our case) and differences between recuperative and non-recuperative cases are around 40%, independently of the season. This is the difference in terms of fuel consumption rate of incorporating a recuperator to pre-heat the working fluid at the compressor exit. When the plant works on a hybrid mode because received irradiance is enough to heat the pressurized air above T_2 (without recuperation) or T_x (with recuperation), the fuel rate saving is important, and obviously depends on seasonal conditions. For each operation mode, the fuel saving for a whole day corresponds to the area of the surface between the solid lines in Fig. 5 (hybrid mode) and the corresponding dashed ones (pure combustion). The results are summarized in Table 2. The legend '*combustion mode*' corresponds to the case of no solar heat input and '*hybrid mode*' to the case in which solar irradiance is enough for partial heat input coming from the central tower solar plant. For the non-recuperative plant the saving varies from 2.8% in winter to 8.5% in summer. Autumn and spring behave in a similar way, the saving is about 5.3%. For the recuperative case relative differences are slightly larger: change from 3.9% in winter to 11.5% in summer. In autumn and spring, now the saving is around 7.3%.

Table 2: Seasonal fuel consumption prediction on the basis of natural gas fueling.

	m_f (ton per day)	Winter	Spring	Summer	Autumn
No recuperation	Combustion mode	31.1	30.8	30.2	29.9
	Hybrid mode	30.3	29.2	27.6	28.3
Fuel saving (%)		2.8	5.3	8.5	5.4
With recuperation	Combustion mode	22.3	22.3	22.1	22.1
	Hybrid mode	21.5	20.6	19.6	20.5
Fuel saving (%)		3.9	7.3	11.5	7.5

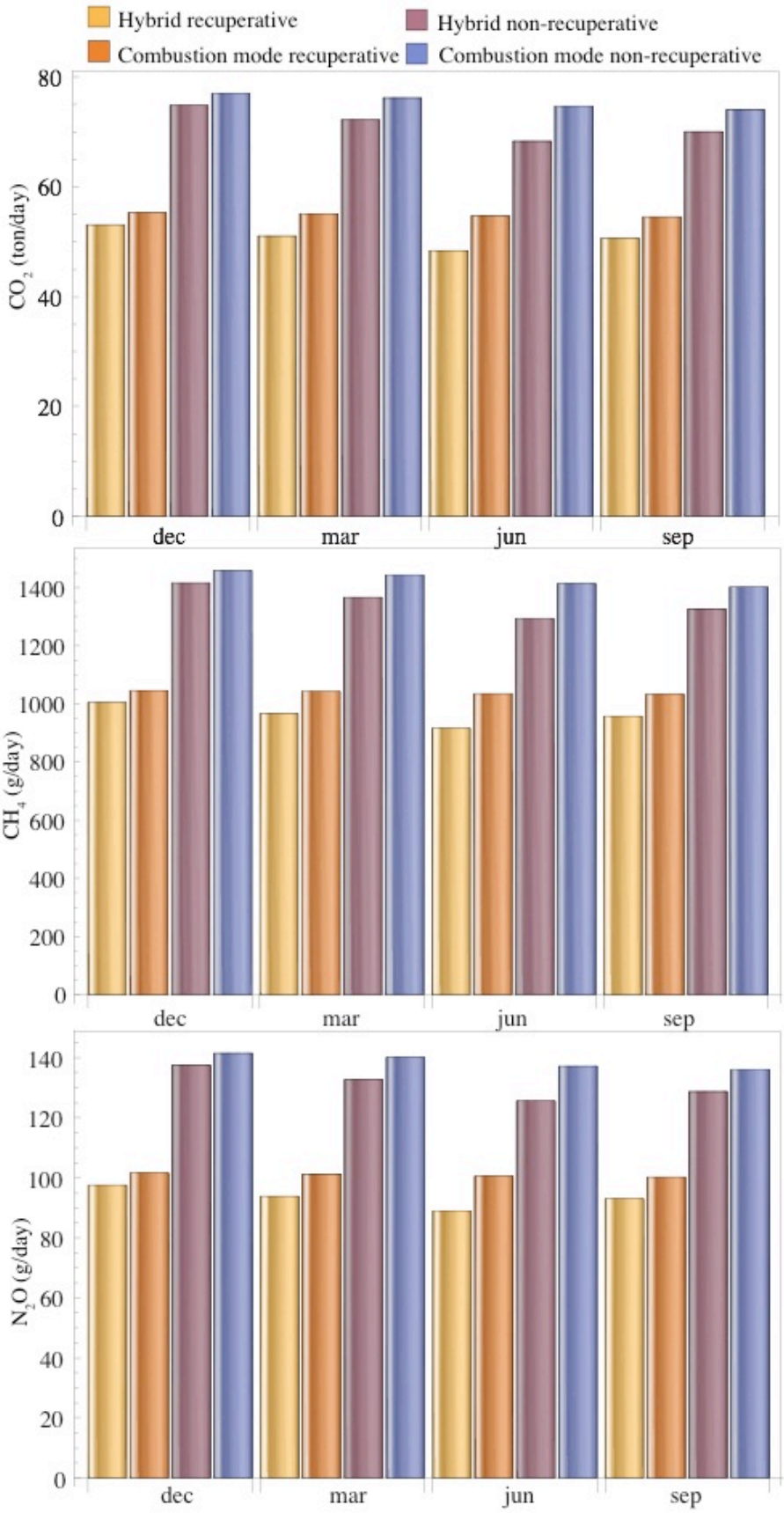

Figure 6: Real units estimation of greenhouse emissions

The differences among plant configurations in fuel consumption are directly transferred to pollutant emissions. As an illustration we have plotted in Fig. 6 a bar diagram with the estimated emissions of

the main greenhouse gases in real units: CO_2, CH_4, and N_2O. The data in the figure should only be taken as a guide, because each plant could have particular technologies to reduce emissions or CO_2 capture mechanisms. The data were obtained from the gas natural emission factors collected in [29, 30]. The figure, in daily basis for the considered particular days of each season, allow to discern two emission levels: the associated to the non-recuperative plant and the one arising from the recuperative one. Differences are substantial as previously commented for fuel consumption. Within these two modes, the reduction associated to solar hybridization and its evolution during the year is also apparent.

5 Summary and conclusions

In this paper we have modeled a solar hybrid power plant based on a gas turbine following a closed Brayton cycle. The plant admit several configurations with or without a heat recuperator and with or without solar heat input. An assumed basic constraint of the plant operation is to keep an almost constant power output in the periods of low solar radiation. The model allows a direct calculation of the dynamic plant operation, with variable solar irradiance and variable external temperature. The hybridization scheme follows a serial or sequential heat input divided in two or three steps. In the non-recuperative configuration a heat exchanger transfers the heat received in a central tower solar collector to the working fluid at the exit of the compressor. Then, a combustion chamber completes the energy input required to have a stationary turbine inlet temperature. If a recuperator is included there exists a previous heating process by using the high temperature of the gas at the turbine exit.

The main emphasis was laid on the thermodynamic model of the Brayton cycle, where all the main irreversibility sources were considered avoiding to introduce a huge number of parameters and allowing to obtain analytical equations for all the thermal efficiencies and power output. For the solar subsystems a simple model was taken. It incorporates heat losses in the solar collector due to to radiation and conduction/convection terms. The optical efficiency is an averaged effective factor. The overall plant efficiency was obtained as a combination of the efficiency of the plant subsystems (solar, combustion, and gas turbine) and the effectivenesses of the heat exchangers connecting subsystems. The SOLUGAS project [5, 17] in Spain was elected as prototypical installation to compare model predictions with. Good agreement between measured values and predicted ones was found.

After the validation in stationary conditions, real seasonal data for solar irradiance and ambient temperature were incorporated to our computational scheme and taking representative days for each season, results were presented. Curves of global plant thermal efficiency, efficiencies of the subsystems, solar share, power output, and fuel conversion rate were shown in hourly basis. All the results are in agreement with other in the literature obtained both from real prototype installations and within simulation frameworks. Explicit data for fuel consumption rate and greenhouse gases inventory were presented and analyzed.

Results show that a recuperative plant working in hybrid mode has a fair potential to generate a stable power output of about 4.6 MW with reduced fuel consumption and reduced greenhouse emissions for a location with favorable insolation conditions. Likely, the high temperature of the working gas at the recuperator exit, make these plants susceptible to be combined with a bottoming cycle, in order to increase global combined efficiency. Hybridization scheme is simple and susceptible to be used in arid regions with low water availability. The framework presented here should be considered as a starting step for the dynamic simulation of this kind of plants within thermodynamic basis. The implementation of more sophisticated models for the solar subsystem is feasible. They could include daily and seasonal variations of optical and other losses and the particularities of the solar collector field. Also more elaborated models for the involved solar receiver and other heat exchangers could be considered as well as optimization analyses based on thermoeconomic criteria for particular plants. Different working fluids for the thermal cycle are also susceptible of analysis.

Acknowledgments

The authors acknowledge financial support from MINECO of Spain, Grant ENE2013-40644-R and University of Salamanca.

References

[1] M. Romero, A. Steinfeld, Concentrating solar thermal power and thermochemical fuels, Energy Environ. Sci. 5 (2012) 9234–9245.

[2] O. Behar, A. Khellaf, K. Mohammedi, A review of studies on central receiver solar thermal power plants, Rene. Sust. Energ. Rev. 23 (2013) 12–39.

[3] P. Schwarzbözl, R. Buck, C. Sugarmen, A. Ring, M. Marcos Crespo, P. Altwegg, J. Enrile, Solar gas turbine systems: design, cost and perspectives, Sol. Energy 80 (2006) 1231–1240.

[4] Solar-hybrid power and cogeneration plants , Tech. rep., European Commission (2011).
URL ordis.europa.eu/publication/rcn/13318 – en.html

[5] R. Korzynietz, M. Quero, R. Uhlig, Solugas-future solar hybrid technology , Tech. rep., SolarPaces (2012). URL http://cms.solarpaces2012.org/proceedings
/paper/7ee7e32ece8f2f8e0984d5ebff9d77b

[6] M. Dunham, B. Iverson, High-efficiency thermodynamic power cycles for concentrated solar power systems, Renew. Sust. Energ. Rev. 30 (2014) 758–770.

[7] G. Barigozzi, A. Perdichizzi, C. Gritti, I. Guaiatelli, Techno-economic analysis of gas turbine inlet air cooling for combined cycle power plant for different climatic conditions, Appl. Therm. Eng. 82 (2015) 57–67.

[8] E. Okoroigwe, A. Madhlopa, An integrated combined cycle system driven by a solar tower: a review, Renew. Sust. Energ. Rev. 57 (2016) 337–350.

[9] B. Grange, C. Dalet, Q. Falcoz, F. Siros, A. Ferrière, Simulation of a hybrid solar gas-turbine cycle with storage integration, Energ. Proc. 49 (2014) 1147–1156.

[10] E. Okoroigwe, A. Madhlopa, Evaluation of the potential for hybridization of gas turbine power plants with renewable energy in South Africa, IEEE Conference Publications, 2015. doi:10.1109/DUE.2015.7102985 .

[11] J. Spelling, Hybrid solar gas-turbine power plants, Ph.D. thesis, KTH Royal Institute of Technology, Department of Energy Technology, Stockholm, Sweden (2013).

[12] Y. Li, S. Liao, G. Liu, Thermo-economic multi-objective optimization for a solar-dish Brayton system using NSGA-II and decision making, Elect. Power. Energ. Sys. 64 (2015) 167–175.

[13] G. Barigozzi, G. Bonetti, G. Franchini, A. Perdichizzi, S. Ravelli, Thermal performance prediction of a solar hybrid gas turbine, Sol. Energy 86 (2012) 2116–2127.

[14] F. Collado, J. Guallar, A review of optimized design layouts for solar power tower plants with campo code, Ren. Sust. Energ. Rev. 20 (2013) 142–154.

[15] R. Soltani, P. Keleshtery, M. Vahdati, M. Khoshgoftar Manesh, M. Rosen, M. Amidpour, Multi-objective optimization of a solar-hybrid cogeneration cycle: application to CGAM problem, Energ. Conv. Manage. 81 (2014) 60–71.

[16] W. Le Roux, T. M. J. Bello-Ochende, A review on the thermodynamic optimisation and model of the solar thermal Brayton cycle, Renew. Sust. Energ. Rev. 28 (2013) 677–690.

[17] D. Olivenza-León, A. Medina, A. Calvo Hernández, Thermodynamic modeling of a hybrid solar gas-turbine power plant, Energ. Convers. Manage. 93 (2015) 435–447.

[18] M. Santos, R. Merchán, A. Medina, A. Calvo Hernández, Seasonal thermodynamic prediction of the performance of a hybrid solar gas-turbine power plant, Energ. Convers. Manage. (2016) Accepted for publication.

[19] S. Sánchez-Orgaz, A. Medina, A. Calvo Hernández, Recuperative solar-driven multi-step gas turbine power plants, Energ. Convers. Manage. 67 (2013) 171–178.

[20] S. Sánchez-Orgaz, M. Pedemonte, P. Ezzatti, P. Curto-Risso, A. Medina, A. Calvo Hernández, Multi-objective optimization of a multi-step solar-driven Brayton cycle, Energ. Convers. Manage. 99 (2015) 346–358.

[21] J. Heywood, Internal Combustion Engine Fundamentals, McGraw-Hill, 1988.

[22] J. Duffie, W. Beckman, Solar Engineering of Thermal Processes, John Wiley and Sons, Hoboken, New Jersey, 2006.

[23] L. Weinstein, J. Loomis, B. Bhatia, D. Bierman, E. Wang, G. Chen, Concentrating solar power, Chem. Rev. 115 (2015) 12797–12838.

[24] S. T. Caterpillar, https://mysolar.cat.com/cda/files /126873/7/dsm50pg.pdf . URL https://mysolar.cat.com/cda/files/126873/7/dsm50pg.pdf

[25] E. W. Lemmon, M. L. Huber, M. O. McLinden, NIST Standard Reference Database 23: Reference fluid thermodynamic and transport properties-REFPROP, version 9.1, National Institute of Standards and Technology, Standard Reference Data Program, Gaithersburg (2013).

[26] M. Romero, R. Buck, E. Pacheco, An update on solar central receiver systems, projects, and technologies, Transactions of the ASME 124 (2002) 98.

[27] GREET, The Greenhouse Gases, Regulated Emissions and Energy Use in Transportation Model. , Tech. rep., Argonne National Laboratory, Argonne, IL (2010). URL http://greet.es.anl.gov

[28] Meteosevilla. http://www.meteosevilla.com . URL http://www.meteosevilla.com

[29] Direct emissions from stationary combustion sources (May 2008). URL www.epa.gov/climateleaders

[30] Emission factors for greenhouse gas inventories (April 2014). URL http://www.epa.gov/climateleadership/documents/emission-factors.pdf